23rd Australasian Fluid Mechanics Conference – 23AFMC
Sydney, Australia
4-8 December 2022 Paper No: AFMC2022-021

Physical Modelling of Compression Wave Impacting Moored Vessel

Hubert Chanson [1]

[1] School of Civil Engineering, The University of Queensland, Brisbane, QLD 4072, Australia

* Email: h.chanson@uq.edu.au

Abstract

When a compression wave of tidal origin forms in a converging estuarine channel with large tidal ranges, its upstream propagation interacts with natural landforms and man-made structures and vessels. The present study was motivated by the well-documented impact of tidal bores on harbours and navigation, although it is also relevant to other industrial processes. Physical modelling was performed in a relatively large-size physical facility. Compression waves were generated in a 19 m long 0.5 m wide channel. Suspended vessels were placed in the channel, and the surge impact on the vessel was documented. Two vessel shapes were tested for a range of hydrodynamic conditions. The experiments were repeated and the quantitative data sets' ensemble statistics were analysed. The results showed a complicated transient process during the initial stages. The compression wave impact was characterised by relatively large horizontal accelerations, associated with an upstream entrainment of the vessel and an upward shift induced by buoyancy effect.

1. Introduction

When a compression wave of tidal origin forms in a converging estuarine channel with large tidal ranges, i.e. a tidal bore, its upstream propagation interacts with natural landforms (river banks, bends, islands, sand bars) as well as man-made structures, harbours, ships and vessels (Figure 1). The tidal bore of the Hoogly River has hindered the navigation to and from the Port of Calcutta for several centuries and has been listed as a hazard in navigation charts and nautical instructions (Bazin 1865, Mazumder and Bose 1995, Chanson 2011). In Burma, the tidal bore of the Sittang River adversely affected navigation during the 19th and 20th centuries (Stuart 1932). Tragedies have been documented for the tidal bores of the Seine River (France), Colorado River (Mexico), Qiantang River (China), Fly and Bamu Rivers (Papua New Guinea) (Sykes 1937, Malandain 1989, Chanson 2011, Pan and Chanson 2015).

Navigation instructions for moored ships were very strict in tidal bore-affected harbours channels, such as Rouen on the Seine River, Bordeaux on the Garonne River, Calcutta on the Hoogly River and Hangzhou on the Qiantang River. Ships were typically instructed to move in the centre of the river channel. In the Qiantang River (China), Moore (1888) presented a shelter for vessels awaiting the bore (Figure1A). After the bore roller impacted the junks, the sailors guided their ships in the strong flood tidal current to sail towards the city of Hangzhou at a speed of up to 10 knots (Tricker 1965).

The present study was motivated by the well-documented impact of tidal bores on vessels, although it is also relevant to sloshing in bulk carrier hulls and overtopping of green waters on offshore structures, large ships and floating, production, storage, and offloading (FPSO) units (Ramsden and Raichlen 1990, Ramsden 1996, Ryu et al. 2007). Herein, detailed physical modelling was performed in a relatively large-size physical facility. Suspended vessels were placed in the channel, and the surge front impact on the vessel was analysed. Two vessel shapes were tested for a range of hydrodynamic conditions. The experiments were systematically repeated and the results showed a complicated transient multiphase fluid-structure process.

Figure 1. Bore shelter for junk at Haining (China) during the 19th century with the incoming breaking bore in the background (after Moore 1888), breaking "bore at the mouth of the Tsien River" about 1903-1906 by Ernst Boerschmann, tidal bore of the Qiantang River at Haining (China) on 7 September 2013, and fishing boat negotiating the Qiantang River at Meilvba, Hangzhou (China) on 12 October 2015.

2. Theoretical considerations

Let us consider a suspended vessel (Figure 2 Left). The force acting on the body at rest are the weight/gravity force W and the traction force T. When a breaking bore propagates upstream past the suspended body (Figure 2 Right), the forces acting on the body encompass the weight/gravity force W, the buoyancy force F_b, the traction force T, the pressure force F_p, the virtual mass force $F_{virtual}$, and the Basset history force F_{basset}. In a vector format, Newton's law of motion applied to the suspended body gives in first approximation.

$$M \times \vec{a} = \vec{W} + \vec{T} + \vec{F_b} + \vec{F_p} + \overrightarrow{F_{virtual}} + \overrightarrow{F_{Basset}} \,, \tag{1}$$

where M is the mass of the body, and a is the acceleration of the body. In Equation (1), the pressure force combines the lift and drag force.

In the longitudinal horizontal x-direction, the forces acting on a body initially at rest in suspension include the traction force's horizontal component T_x = $T \times \sin\theta$, the pressure force component $(F_p)_x$, a virtual mass force $F_{virtual}$, and the Basset history force F_{Basset}. The Basset history force term is small when the body is initially at rest. Thus, the application of Newton's law of motion in the horizontal direction gives:

$$M \times a_x = T \times \sin\theta - (F_p)_x + \frac{M_{sub}}{s} \times C_m \times \frac{\partial (V_x + U)}{\partial t} \,, \tag{2}$$

where a_x is the longitudinal acceleration component positive downstream, V_x is the velocity component of the body, x is positive downstream, M_{sub} is the mas of the submerged body section, s is the submerged body section's relative density, U is the bore roller celerity, i.e. assuming implicitly that the fluid velocity in the roller front equals the bore celerity, positive upstream, q is the angle between the traction force and horizontal (Figure 2), and C_m is an added mass coefficient. In the vertical direction, Newton's law of motion yields:

$$M \times a_z = T \times \cos\theta - W + F_b + (F_p)_z - \frac{M_{sub}}{s} \times C_m \times \frac{\partial V_z}{\partial t}, \tag{3}$$

By analogy with wave and wind flows, the fluid force acting in the horizontal direction may be calculated from a general form of the Morison's equation (e.g. Apelt and Piorewicz 1987):

$$F_x = -\frac{1}{2} \times \rho \times C_D \times A \times (V_x + U) \times |V_x + U| + \frac{M_{sub}}{s} \times C_m \times \frac{\partial (V_x + U)}{\partial t}, \tag{4}$$

with ρ the fluid density, A is the projected submerged area, and C_D a drag coefficient.

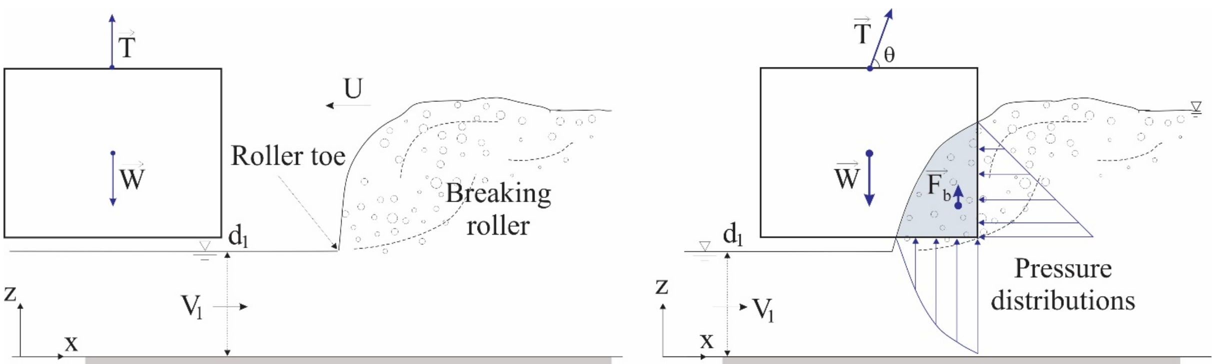

Figure 2. Schematic of a breaking bore impacting a suspended breakwater/caisson, with bore propagation from right to left, prior to impact (Left) and during impact (Right).

3. Experimental facility and procedure

3.1 Experimental flumes, physical models and instrumentation

New experiments were conducted in a 19 m long 0.7 wide rectangular tilting channel at the University of Queensland. The initially-steady water flow was supplied by an upstream intake structure designed to deliver smooth inflow conditions into the channel, and equipped with baffles, flow straighteners and a smooth convergent intake. A fast-closing Tainter gate was located next to the downstream end of the channel at x = 18.1 m, where x is a longitudinal distance from the upstream end of the channel.

Two different moored vessels were built: a caisson model and a barge model (Figure 3). The caisson model was made out of perspex, with a 0.450 m × 0.2 m rectangular base and, its mass was 2.55 kg. The caisson model was moored at x = 10.5 m and 0.02 m away from the right sidewall. The caisson model was located close to glass side wall to observe the impact from the side view, and it was held with four strings. The barge model was made of expanded polystyrene, with a height of 0.055 m, a top length of 0.450 m, with 1V:5H swimming ends, a bottom width of 0.25 m, a 0.15 m width and a total mass of 0.4 kg. It was moored at x = 9.8 m in the middle of the channel width, to study from both side and top views. The barge model was held with two strings. Both models were initially suspended 0.005 m above the initially-steady water free-surface, i.e. they did not interact with the initially-steady flow.

The initial water discharge was measured using a magneto-flowmeter with an accuracy of less than 2%. The roller toe perimeter, roller's water surface, vessel motion were recorded with a digital camera Sony™ DSC-RX100VA operating at 30 fps in 4K movie mode. Further observations were conducted with a dSLR camera Pentax™ K-3 equipped with full-frame prime lenses (Figs. 4, 5 & 6).

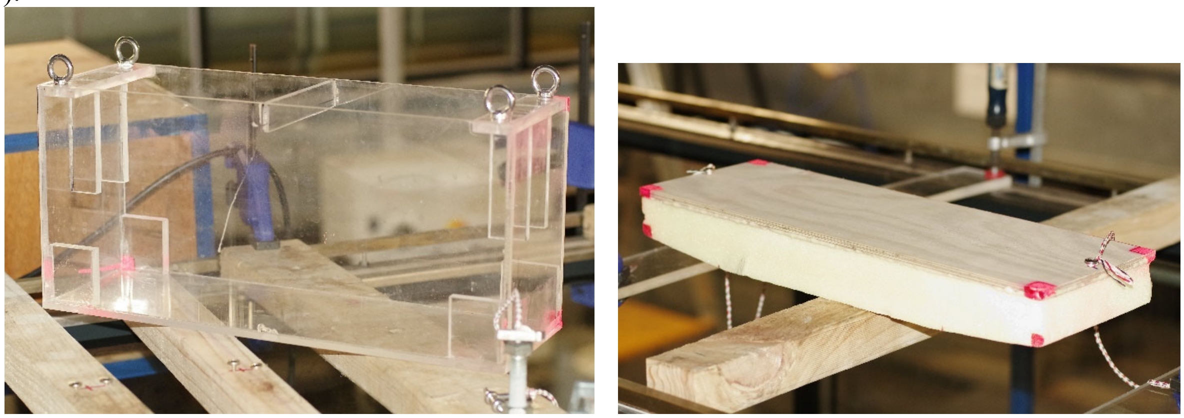

Figure 3. Physical models of caisson and barge. For scale, the timber supporting the models is identical in both photographs.

3.2 Experimental flow conditions

Visual, photographic and cinematographic observations were conducted for four initial flow conditions (Table 1). Detailed measurements were undertaken for the flow condition K1 (Table 1). In each case, the tidal bore was generated by the rapid and complete closure of the Tainter gate. The compression wave propagated upstream and all observations stopped once the surge reached the upstream intake structure. The Tainter gate closure time was less than 0.15-0.2 s, and the short closure time was small enough to have a negligible effect on the bore propagation. The compression wave's Froude number was controlled by the initial flow depth d_1 and bed slope S_o.

Test	S_o	Q (m^3/s)	d_1 (m)	U (m/s)	Fr_1	Re
K1	0.0132	0.101	0.085	0.7	2.6	2×10^5
Y1		0.10	0.082	0.49	2.5	1.8×10^5
Y2		0.046	0.049	0.30	2.38	0.8×10^5
Y3		0.058	0.058	0.35	2.4	1×10^5

Table 1. Experimental flow conditions. Notation: d_1: initial water depth; U = bore celerity; Fr_1 = bore Froude number; Re = bore Reynolds number; S_o: invert slope.

4. Basic flow features

For all investigated flow conditions (Table 1), the incoming compression wave was a bore with a breaking roller. Figures 4 (Top), 5 (Top) and 6 (Top) show the roller just before impact. The bore advanced as a hydraulic jump in translation, with a celerity U ≈ 0.7 m/s in average. However, the propagation was a highly turbulent and fluctuating process. A key feature was the strong aeration of the bore roller. In particular, all observations showed a very strong aeration of the bore's leading edge, as previously reported for slightly different flow conditions (Leng and Chanson 2019).

With the caisson model, the roller impact initially induced a horizontal thrust with increasing acceleration over the first half second (Figure 5, 2nd from top). This was followed by a rotating motion, with horizontal axis perpendicular to the sidewall, as the downstream end of the barge moved upwards (Figure 5, 3rd from top). The upward motion of the downstream end of vessel was driven by buoyancy because the downstream bottom corner became submerged, while the vessel was dragged also by the bore front, as a result of the pressure force acting on the downstream face of the caisson. With increasing time, the entire caisson model was pushed upwards by buoyancy, when all bottom corners became submerged (Figure 5, bottom).

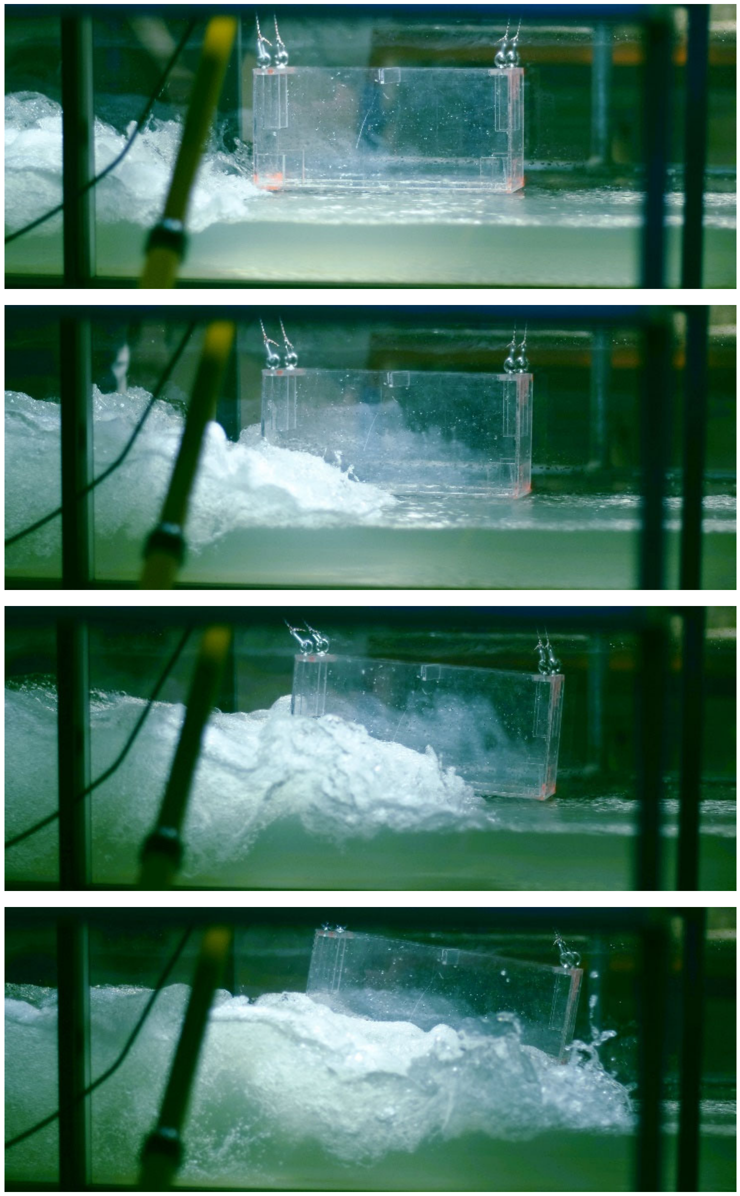

Figure 4. Compression wave impact on caisson model. Flow conditions: $Fr_1 = 2.6$, $Re = 2\times10^5$; compression wave propagation from left to right; 0.36 s between successive frames (from top to bottom). Shutter speed: 1/250 s.

The barge model motion was somehow different from the caisson model. Although the initial motion and horizontal thrust was the same for both vessels (Figs. 4 & 5, 2nd from top), the barge model rode quickly at the roller surface, as a direct result of the roller impact on the 1V:5H swimming end (Figure 5, 3rd from top). This was consistent with the shape of fishing boats negotiating the Qiantang River bore (Figure 1, Bottom right). For completeness, initial tests were conducted with a rectangular barge model without swimming ends, during which the rectangular barge model became completely submerged by the roller.

5. Vessel kinematics: preliminary results

The vessel motion was recorded with relatively high speed movies (100 fps) and the corners were tracked using the software Tracker v. 4.91, operating in a semi-automatic mode. The trajectory data of the vessel's outer corners were differentiated using a 7-point stencil central difference method to yield the velocity and acceleration. The experiment (K1) was repeated 5 times and the data set's ensemble median was calculated.

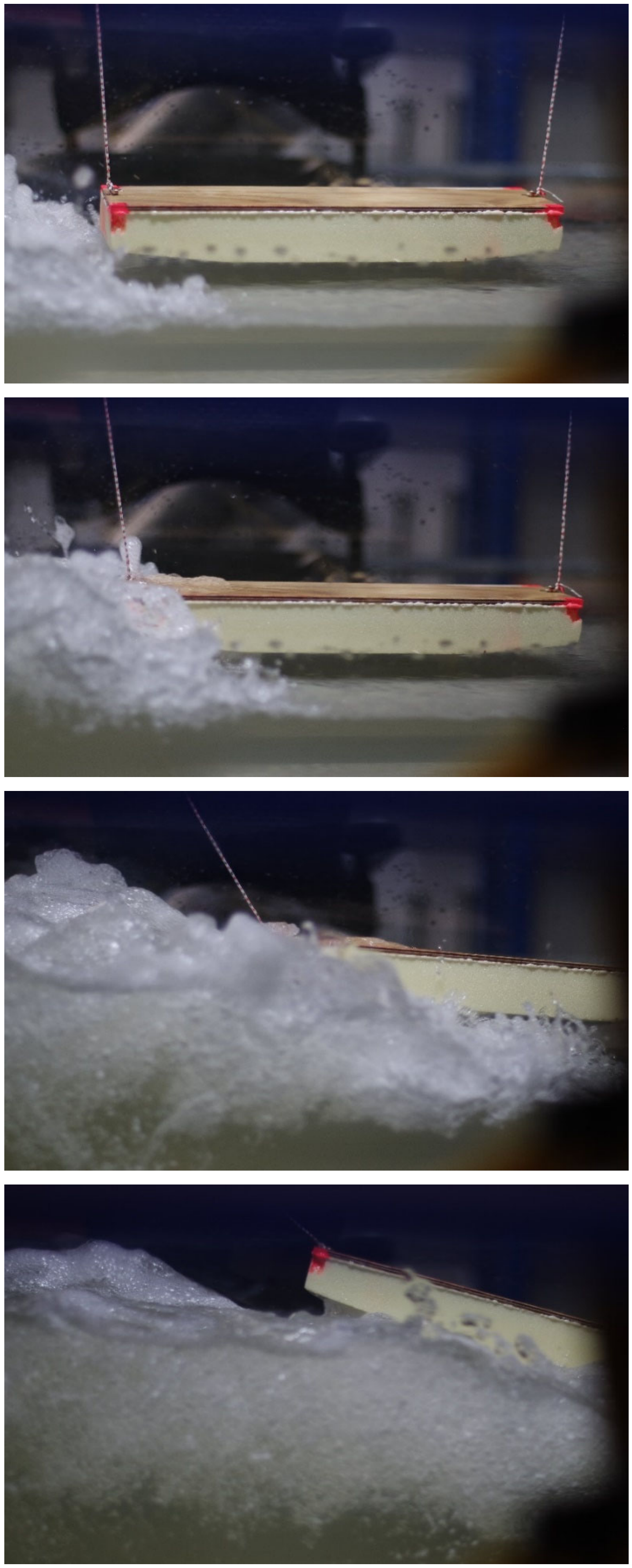

Figure 5. Compression wave impact on barge model. Flow conditions: $Fr_1 = 2.6$, $Re = 2\times10^5$. Compression wave propagation from left to right. t' = 0, 0.24 s, 0.84 s, 1.57 from top to bottom. Shutter speed: 1/250 s.

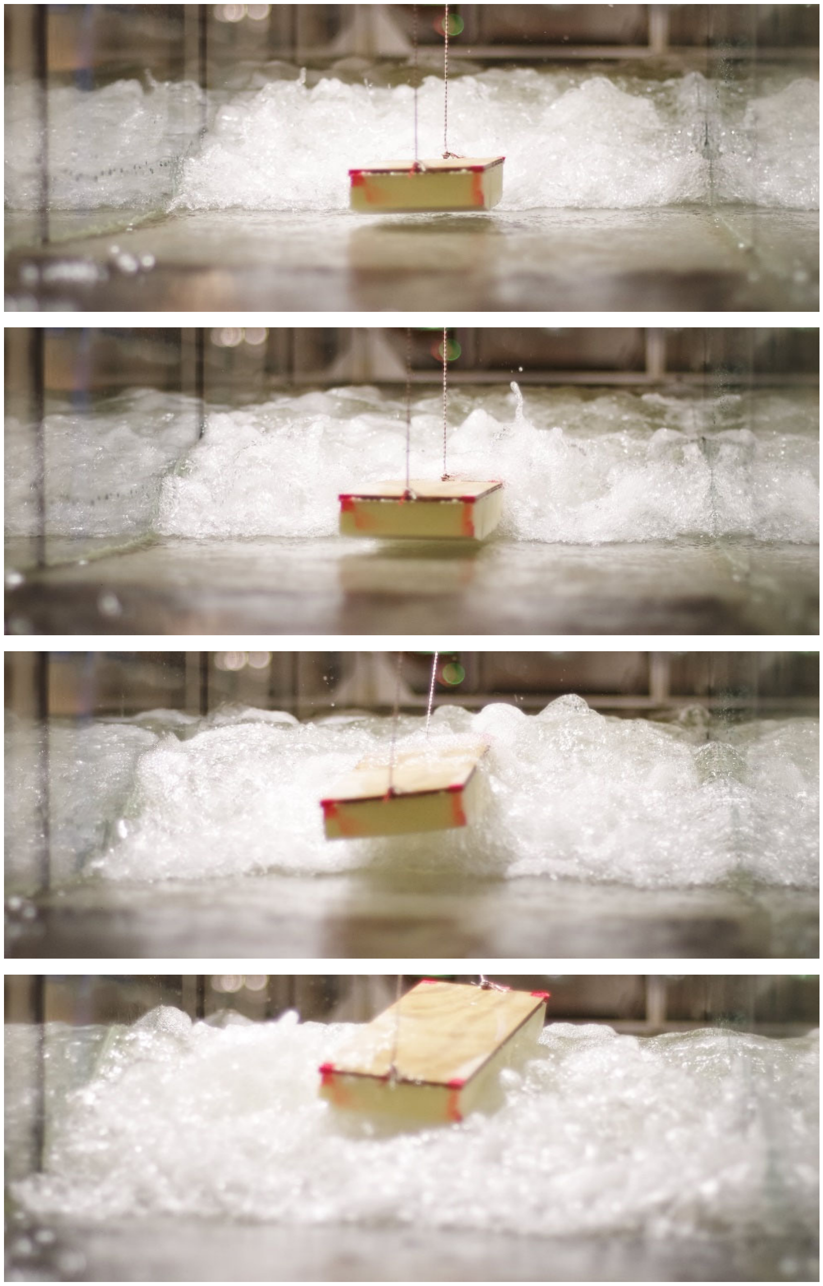

Figure 6. Compression wave impact on barge model. Flow conditions: $Fr_1 = 2.6$, $Re = 2\times10^5$. Compression wave propagation from background to foreground. t' = 0, 0.24 s, 0.84 s, 1.57 from top to bottom. Shutter speed: 1/250 s.

The instantaneous vessel velocity data ranged from 0 to 0.2 m/s typically, although a few outliers were seen (Song 2021). Basically, the vessel's maximum velocity was substantially smaller than the bore celerity ($U \approx 0.7$ m/s) during the experiments with the caisson and barge models. Further the vessel velocity fluctuations were substantially smaller than the bore celerity fluctuations before impact, owing to the inertia of the vessels.

The maximum ensemble median acceleration amplitude was about 4 m/s^2 for the caisson model and about 3 m/s^2 for the barge model during the experiment K1. The differences may be attributed to differences in inertia, shape and string attachments between the two models. All the instantaneous acceleration time series however presented large fluctuations, linked to sudden and rapid changes in instantaneous vessel velocity with time.

6. Conclusion and future directions

The impact of compression waves on suspended vessels was tested experimentally in a 19 m long 0.5 m wide flume. Two vessels were used: a rectangular caisson and a barge with swimming ends. A range of flow conditions were applied corresponding to a compression wave with a marked breaking roller.

Although the observations showed an initial horizontal motion of both vessels, the ensuing motion differed between the two vessels. The barge model tended to ride above the roller free-surface, while the caisson model induced a marked disturbance on the flow. Following the impact of compression wave, the instantaneous vessel velocities were significantly less than the bore celerity, and the maximum vessel ensemble median acceleration was less than 0.5×g, with g the gravity acceleration.

Future research should use faster camera to record the vessel motion, while force gauge should be installed on the vessel suspension cables, with pressure sensors on the vessel faces.

Acknowledgments

The author acknowledges the assistance of his student Mr Ki-sub Song for some experimental work, as well as the help of Dr Rui Shi (The University of Queensland), and the technical assistance of Jason Van Der Gevel and Stewart Matthews (The University of Queensland).

References

Bazin, H. (1865). "Recherches Expérimentales sur la Propagation des Ondes." ('Experimental Research on Wave Propagation.') *Mémoires présentés par divers savants à l'Académie des Sciences*, Paris, France, Vol. 19, pp. 495-644 (in French).

Chanson, H. (2011). "*Tidal Bores, Aegir, Eagre, Mascaret, Pororoca: Theory and Observations*." World Scientific, Singapore, 220 pages.

Malandain, J.J. (1988). "La Seine au Temps du Mascaret." (‘The Seine River at the Time of the Mascaret.’) *Le Chasse-Marée*, No. 34, pp. 30-45 (in French).

Mazumder, N.C., and Bose, S. (1995). "Formation and Propagation of Tidal Bore." *Jl of Waterway, Port, Coastal and Ocean Engrg.*, ASCE, Vol. 121, No. 3, pp. 167-175.

Moore, R.N. (1888). "*Report on the Bore of the Tsien-Tang Kiang*." Hydrographic Office, London.

Pan, D.Z., and Chanson, H. (2015). "Physical Modelling of Tidal Bore Dyke Overtopping: Implication on Individuals' Safety." *Proc. 36th IAHR World Congress*, The Hague, The Netherlands, 27 June-3 July, Theme 4, pp. 3824-3831.

Ramsden, J.D. (1996). "Forces on a Vertical Wall due to Long Waves, Bores, and Dry-Bed Surges." *Journal of Waterway, Port, Coastal, and Ocean Engineering*, ASCE, Vol. 122, No. 3, pp. 134-141.

Ramsden, J.D., and Raichlen, F. (1990). "Forces on Vertical Wall caused by Incident Bores." *Journal of Waterway, Port, Coastal, and Ocean Engineering*, ASCE, Vol. 116, No. 5, pp. 592-613.

Ryu, Y., Chang, K.A., and Mercier, R. (2007). "Runup and Green Water Velocities due to Breaking Wave Impinging and Overtopping." *Experiments in Fluids*, Vol. 43, pp. 555-567 (DOI: 10.1007/s00348-007-0332-0).

Song, K.S. (2021). "Physical Modelling of the Impact of Breaking Surges on Moored Vessels." *CIVL4560 Project Report*, The University of Queensland, School of Civil Engineering.

Stuart, J.M.B. (1932). "The Sittang River and Its Vagaries. " *Selected Engineering Papers*, Institute of Civil Eng., London, No. 127, pp. 3-16 & 3 figures.

Sykes, G. (1937). "*The Colorado Delta*." Carnegie Institution of Washington, Publ. No. 460, Baltimore, USA, 193 pages and 1 map.

Tricker, R.A.R. (1965). "*Bores, Breakers, Waves and Wakes*. " American Elsevier Publ. Co., New York, USA.